JACS
JOURNAL OF THE AMERICAN CHEMICAL SOCIETY
pubs.acs.org/JACS
Article

Anionic Templates Drive Conversion between a $Zn^{II}_9L_6$ Tricapped Trigonal Prism and $Zn^{II}_6L_4$ Pseudo-Octahedra

Hua-Kui Liu, Tanya K. Ronson, Kai Wu, Dong Luo, and Jonathan R. Nitschke*

Cite This: J. Am. Chem. Soc. 2023, 145, 15990−15996
Read Online
ACCESS | Metrics & More | Article Recommendations | Supporting Information

ABSTRACT: This work introduces the use of 8-aminoquinoline subcomponents to generate complex three-dimensional structures. Together with a tris(formylpyridine), 8-aminoquinoline condensed around Zn^{II} templates to produce a tris(tridentate) ligand. This ligand is incorporated into either a tricapped trigonal prismatic $Zn^{II}_9L_6$ structure or a pair of pseudo-octahedral $Zn^{II}_6L_4$ diastereomers, with S_4 and D_2 symmetries. Introduction of a methyl group onto the aminoquinoline modulated the coordination sphere of Zn^{II}, which favored the $Zn^{II}_9L_6$ structure and disfavored the $Zn^{II}_6L_4$ assembly. The tricapped trigonal prismatic $Zn^{II}_9L_6$ architecture converted into a single $Zn^{II}_6L_4$ cage diastereomer following the addition of a dianionic 4,4′-dinitrostilbene-2,2′-disulfonate guest. Four of these guests clustered tightly at the four windows of the $Zn^{II}_6L_4$ cage, held in place through electrostatic interactions and hydrogen bonding, stabilize a single diastereomeric configuration with S_4 symmetry.

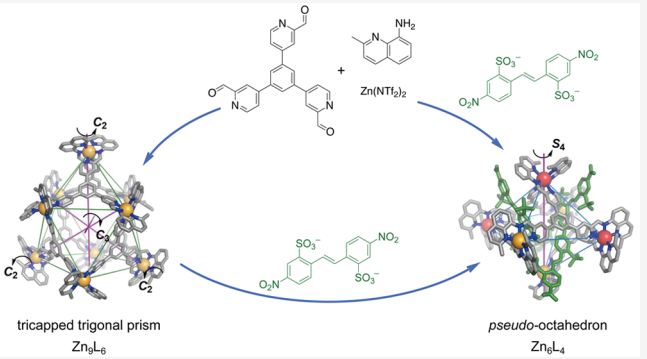

INTRODUCTION

Three-dimensional coordination cages with well-defined enclosed cavities have found applications in stabilizing reactive species,[1,2] binding and sensing guests,[3] chemical separations,[4] and catalyzing reactions.[5] The subcomponent self−assembly strategy has enabled the preparation of many metal−organic capsules from simple building blocks, as intricate products form from amine and aldehyde precursors together with metal ions via the concurrent formation of dynamic coordinative and reversible covalent imine bonds.[6]

Cages such as tetrahedra,[7] cubes,[8] and octahedra[9−11] have thus been prepared. These high-symmetry cages contain pseudo-spherical cavities,[12] which enable them to bind approximately spherical guests. Metal−organic cages with lower symmetry[13] could enable the binding of non-spherical guests, such as biomolecules and pharmaceuticals. For example, a triangular prismatic architecture with an anisotropic cavity is capable of binding a series of asymmetric drugs and natural products.[14] Clever and co-workers used a low-symmetry bowl-shaped metal−organic cage[15] to act as a supramolecular mask of bound C_{60}, to effect mono-functionalization of the fullerene on its unprotected face, rather than the bi-functionalization that occurs within a cubic coordination cage or a metal−organic framework.[16] New methods of preparing low-symmetry cages are thus very much worth pursuing.

Methods that have been developed to construct low-symmetry cages[13] include the use of low-symmetry or flexible ligands,[17] solvent effects,[18] the use of anions and other templates,[9f,19] heteroleptic architectures,[14] and multimetallic assemblies.[20] However, creating low-symmetry cages by engineering the stereochemistry of metal vertices has proven challenging.[21] M_6L_4 architectures with different C_2-symmetric vertices (Table S1) usually display high symmetry, with rare exceptions.[22] We hypothesized that the coordination-vector geometry of tris(tritopic) ligands shown in Figure 1 would lead to the generation of a new class of M_6L_4 cages, where steric hindrance within a ligand (Table S2) might lead to the formation of a lower-symmetry cage, and clashes between ligands may favor the formation of higher-nuclearity structures. The formation of structures **1** and **2** (Figure 1) supported these hypotheses, as detailed below.

Here, we report the preparation of two novel types of low-symmetry metal−organic cage structures—a $Zn^{II}_9L_6$ tricapped trigonal prism, and two $Zn^{II}_6L_4$ architectures with octahedral metal-ion frameworks, but S_4 and D_2 point symmetries, assembled from the same tris(formylpyridine) subcomponent **A** (Figure 1) under different reaction conditions. The $Zn^{II}_9L_6$ architecture, which is not among the more commonly observed Archimedean and Platonic solids, converts into a S_4-symmetric

Received: April 17, 2023
Published: July 13, 2023

https://doi.org/10.1021/jacs.3c03981
J. Am. Chem. Soc. 2023, 145, 15990−15996

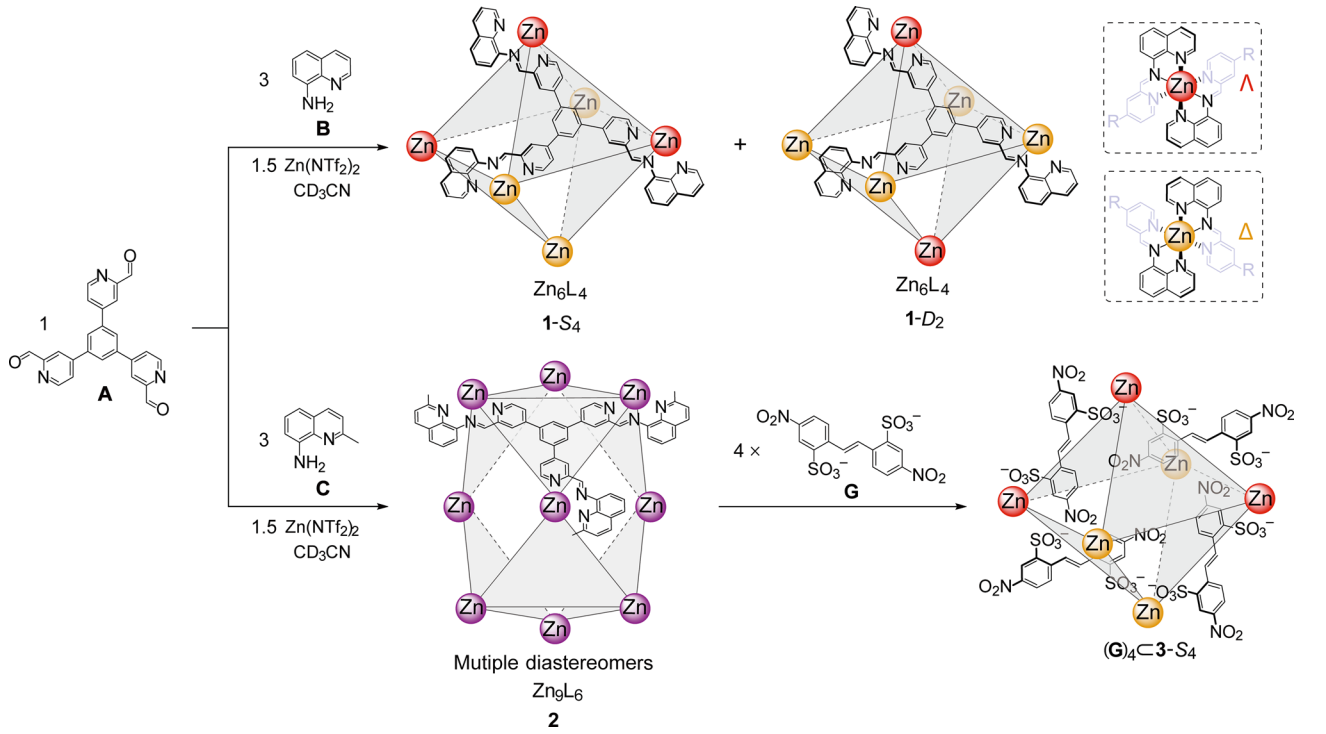

Figure 1. Subcomponent self−assembly of $Zn^{II}_6L_4$ **1** and $Zn^{II}_9L_6$ **2** and the guest-templated conversion of **2** to $(\mathbf{G})_4\subset\mathbf{3}$-$S_4$. Δ and Λ metal stereoconfigurations are shown in yellow and red, respectively.

$Zn^{II}_6L_4$ cage through the action of disulfonate templates (Figure 1).

RESULTS AND DISCUSSION

Self−Assembly of $Zn^{II}_9L_6$ and $Zn^{II}_6L_4$ Metal−Organic Cages. Subcomponent **A** was prepared through Suzuki−Miyaura cross-coupling of 1,3,5-tris(4,4,5,5-tetramethyl-1,3,2-dioxaborolan-2-yl) benzene and 4-bromopicolinaldehyde (see Supporting Information Section 2). The reaction of **A** (4 equiv) and 8-aminoquinoline **B** (12 equiv) with zinc(II) bis(trifluoromethanesulfonyl)imide (triflimide or NTf_2^-, 6 equiv) in CD_3CN at 70 °C resulted in the formation of $Zn^{II}_6L_4$ cage **1**. HR−ESI−MS showed a sharp set of peaks, corresponding to charge states from +8 to +4, all of which confirmed a $Zn^{II}_6L_4$ composition (Figures S15 and S16).

The ^{1}H NMR spectrum of **1** contained two sets of ligand signals in a 2:1 ratio (Figure 2b). Three magnetically distinct chemical environments for the ligand protons of **1** were observed, in a 1:1:1 integrated ratio. The ^{1}H NMR diffusion-ordered spectrum (DOSY) of **1** showed that all of its signals had the same diffusion coefficient of 4.05×10^{-6} cm^2 s^{-1} (Figure S10), consistent with the formation of multiple diastereomeric species with a common size of 3.0 nm modeled using the PM7[23] force field of Scigress[24] (Figure S64). All of the protons of **1** were assigned using different two-dimensional NMR techniques (Figures S8, S11, and S12).

We sought to elucidate the configurations adopted by cage **1** through NMR analysis. The ligands adopt configurations with different torsions between the central phenyl and peripheral pyridine rings to minimise ring eclipsing, similar to, but less regular than, the propeller-like configurations observed in higher-symmetry structures.[25] Geometrical analysis of cage **1** reveals six enantiomeric pairs of diastereomers, with distinct point symmetries: Δ_6/Λ_6, T; $\Delta_5\Lambda/\Delta\Lambda_5$, C_2; $\Delta_4\Lambda_2/\Delta_2\Lambda_4$, C_1; $\Delta_4\Lambda_2/\Delta_2\Lambda_4$, D_2; $\Delta_3\Lambda_3$, C_3; and $\Delta_3\Lambda_3$, S_4. These stereoisomers are shown in Figure S64.

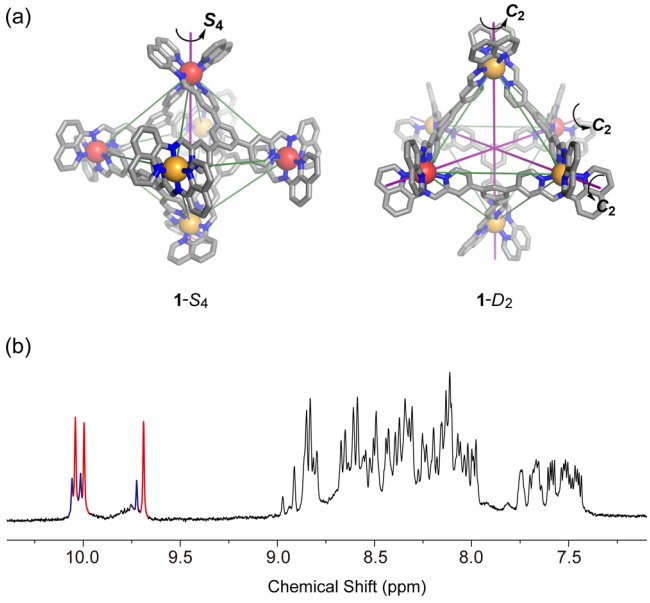

Figure 2. (a) PM7-optimized structure of the S_4 and D_2 diastereomers of cage **1**. Color scheme: Δ-Zn, yellow; Λ-Zn red. (b) ^{1}H NMR spectrum (400 MHz, 298 K, CD_3CN) of cage **1**. The two sets of imine peaks with a 1:1:1 integration ratio are highlighted.

M_6L_4 cages with T point symmetry[11] afford ^{1}H NMR spectra with only one set of ligand peaks, whereas such cages with reduced symmetry, *e.g.*, with C_2, C_1, C_3, S_4, or D_2 point symmetry, are predicted to give rise to spectra with 6, 12, 4, 3, or 3 imine singlet peaks, respectively. Because the ^{1}H NMR spectrum of **1** exhibited two sets of three 1:1:1 imine singlet

https://doi.org/10.1021/jacs.3c03981
J. Am. Chem. Soc. 2023, 145, 15990−15996

peaks (Figure 2b), we inferred that **1** existed in solution as a mixture of diastereomers with S_4 and D_2 symmetries.

To confirm this conclusion, energy minimization of the six stereoisomers was carried out at the PM7[23] level of theory (Figure S64 and Tables S8–S13) using Scigress.[24] Although the calculated energies of these isomers were similar, the **1**-S_4 and **1**-D_2 diastereomers adopted larger dihedral angles between the ligand phenylene and pyridyl rings, which are closer to the values adopted by the free ligand, than for the other four isomers (Table S6). We infer that the larger dihedral angles may favor the **1**-S_4 and **1**-D_2 diastereomers, because in these diastereomers, the steric eclipsing of phenylene and pyridyl hydrogen atoms on the same ligand is reduced. These dihedral angles in the PM7-optimized model of **1**-S_4 are similar to those observed in the crystal structure of **3**-S_4 (Table S6, entries 6–7), and the Zn···Zn separations are similar between model and structure, further suggesting that the S_4 diastereomer of **1**, and its D_2-symmetry analog, with larger dihedral angles according to the model, are energetically favored. We thus conclude that torsional steric hindrance of our new ligand, combined with the coordinate geometry of its vertices, led to the formation of M_6L_4 cages with D_2 and S_4 point symmetries, rather than the higher-symmetry pseudo-octahedra (Table S2).

As concentration dictates the formation of cages with different nuclearities according to Le Chatelier's principle, we hypothesized that increasing the concentration might favor the conversion of a smaller cage into a larger one. Indeed, when the total concentration of **A** was increased from 0.5 to 2.0 mM during the synthesis of **1**, a new species with a $Zn^{II}_9L_6$ composition was detected by HR–ESI–MS alongside $Zn^{II}_6L_4$ **1**. To promote the selective formation of $Zn^{II}_9L_6$ **2**, we sought to modulate the coordination sphere of Zn^{II} through methylation α to the quinoline nitrogen atom of subcomponent **B**. The analysis of models using the PM7[23] force field of Scigress[24] (Table S7) suggests that the introduction of such a methyl group would favor the formation of $Zn^{II}_9L_6$ cage **2** over $Zn^{II}_6L_4$ cage **1**. Thus, the assembly of subcomponent 2-methyl-8-aminoquinoline **C** (18 equiv) together with **A** (6 equiv) and $Zn^{II}(NTf_2)_2$ (9 equiv) at [**A**] = 5.0 mM resulted in the formation of $Zn^{II}_9L_6$ **2** as the uniquely observed product.

The ^{1}H NMR spectrum of **2** (Figure S17) was complex, with many signals, which we ascribe to the presence of multiple diastereoisomers. The ^{1}H DOSY spectrum of **2** (Figure S19) indicated that all signals assigned to cage diastereomers had the same diffusion coefficient, consistent with the formation of isomers with similar sizes. The complex ^{1}H NMR spectrum was assigned using different two-dimensional NMR techniques (Figures S20–S23). The construction of $Zn^{II}_9L_6$ cage **2** is thus enabled through a detailed understanding of the subtle steric effects of the aminoquinoline methyl groups and the phenylene-pyridine torsion angles (Table S6).

Anionic Templates Drive Conversion of $Zn^{II}_9L_6$ to $Zn^{II}_6L_4$. The $Zn^{II}_6L_4$ and $Zn^{II}_9L_6$ frameworks of coordination cages **1** and **2** have distinct geometries, which imply different guest-binding preferences. We hypothesized that the conversion between these frameworks might be achieved following the addition of a suitable guest. Therefore, the use of anionic guests as templates (Figure S26) was investigated to effect the guest-induced conversion from $Zn^{II}_9L_6$ **2** to $Zn^{II}_6L_4$ **3**, an analogue of cage **1** that incorporated methylated **C** instead of **B**.

Complete conversion of $Zn^{II}_9L_6$ **2** to the octahedral $Zn^{II}_6L_4$ framework of **3** occurred after the addition of anionic metal cluster $[PO_4(WO_3)_{12}]^{3-}$ in CD_3CN. The NMR spectra of **3** were complex (Figure S27), suggesting the presence of multiple diastereomers. However, HR–ESI–MS showed only peaks corresponding to the $[PO_4(WO_3)_{12}]^{3-}$ adduct of **3** (Figures S28 and S29). The addition of **G** (**G** = 4,4′-dinitrostilbene-2,2′disulfonate) to $Zn^{II}_9L_6$ **2** in acetonitrile, in contrast, led to complete conversion of **2** to $(\mathbf{G})_4\subset\mathbf{3}$ after 6 h,[26] as confirmed by HR–ESI–MS (Figures S38 and S39). The conversion of **2** to $(\mathbf{G})_4\subset\mathbf{3}$ in dilute solution was accelerated due to the poor solubility of **G** and $(\mathbf{G})_4\subset\mathbf{3}$ (Figures S40–S42). NMR spectra (Figures 3b and S31–S37) indicated the formation of a single isomer with either S_4 or D_2 symmetry, as reflected in the presence of only three imine peaks in a 1:1:1 integral ratio. DOSY confirmed that all the ligand and guest peaks exhibited a single diffusion rate (Figure 3b).

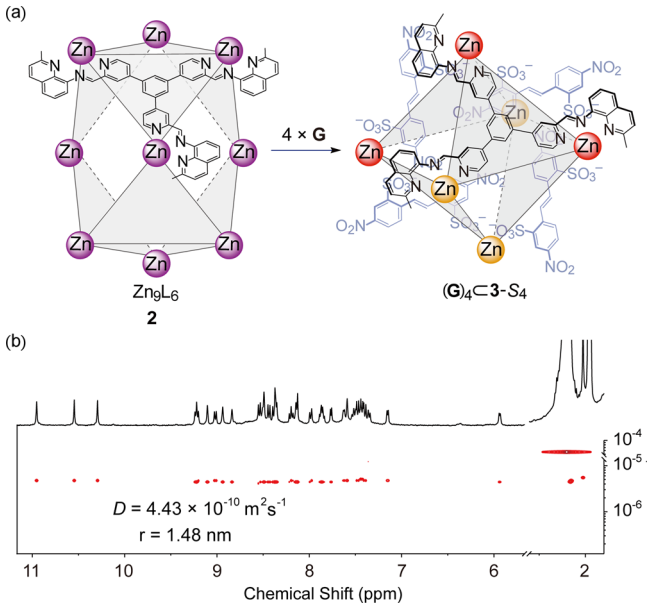

Figure 3. (a) Guest-templated transformation of **2** into $(\mathbf{G})_4\subset\mathbf{3}$-$S_4$. (b) ^{1}H DOSY NMR spectrum (400 MHz, 298 K, CD_3CN) of $(\mathbf{G})_4\subset\mathbf{3}$-$S_4$. **G** = 4,4′-dinitrostilbene-2,2′-disulfonate.

Vapor diffusion of diethyl ether into an acetonitrile solution of $(\mathbf{G})_4\subset\mathbf{3}$ containing $KSbF_6$ resulted in the formation of cube-shaped yellow crystals.[27] Single-crystal X-ray diffraction analysis revealed the solid state structure of $(\mathbf{G})_4\subset\mathbf{3}$ (Figure 4), having an S_4 symmetry consistent with the NMR spectrum recorded in solution (Figure 3b). Inspection of the structure revealed three of the Zn^{II} centers to have Δ handedness, with the other three adopting Λ handedness, lending the capsule achiral S_4 point symmetry. Each metal center is thus related by the S_4 symmetry operation (Figure 4) to a metal center of the opposite stereochemical configuration.

We infer the structure of $(\mathbf{G})_4\subset\mathbf{3}$ to be stabilized by electrostatic attraction and hydrogen bonding (Figure S43) between the cationic cage framework and the anionic guests. Each guest occupies an open face of the octahedral host framework, with each sulfonate group oriented toward a Zn^{II} center. This arrangement thus appears to stabilize the octahedral $Zn^{II}_6L_4$ **3** framework with respect to the larger tricapped trigonal prismatic $Zn^{II}_9L_6$ **2**.

Structures having an octahedral metal framework but lower symmetry are rare;[22] other M_6L_4 octahedra are observed to

https://doi.org/10.1021/jacs.3c03981
J. Am. Chem. Soc. 2023, 145, 15990–15996

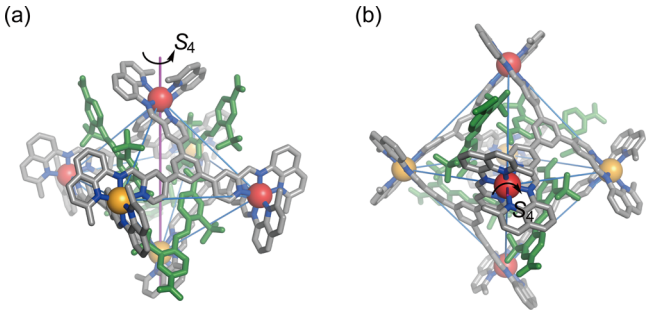

Figure 4. X-ray crystal structure of host–guest complex $(\mathbf{G})_4\subset\mathbf{3}$-$S_4$. (a) View orthogonal to the S_4 axis, showing the compression of the octahedral framework along this axis. (b) View down the S_4 axis, showing the equatorial expansion of the framework. Color scheme: Δ-Zn, yellow; Λ-Zn, red; guest, green; S_4 axis, purple. Ligand nitrogen atoms are blue, and the carbon atoms are gray.

adopt O_h,[9] T_d,[10] or T[11] symmetry. The complex $(\mathbf{G})_4\subset\mathbf{3}$-$S_4$ displayed antipodal metal···metal distances of 20.6 and 16.1 Å, with the Zn^{II} centers on the S_4 axis more closely spaced. We infer this axial compression and equatorial expansion to result from the reduced steric eclipsing of the phenylene and pyridyl hydrogen atoms within ligands, as compared to diastereomers with C_1, C_2, C_3, and T configurations, as supported by PM7 calculations[23] (Table S6). The dihedral angles between the chelate planes of two imino-quinoline moieties coordinated to each Zn^{II} center range from 84–88°.

Host–Guest Chemistry of $Zn^{II}_6L_4$. The complex NMR spectra of $Zn^{II}_9L_6$ cage **2** hampered studies of its host–guest chemistry. We thus focused upon the host–guest chemistry of cage **1**. To determine the binding stoichiometry and affinities for different guests, we performed titration experiments by ^{1}H NMR spectroscopy. Job plots[28] of the titration of $B(p\text{-}C_6H_4Cl)_4^-$ into a solution of **1** were consistent with a 1:4 host–guest binding ratio (Table 1, and Figures S44 and S45).

Table 1. Summary of the Binding Constants of Anionic Guests to Cage 1

guest	volume (Å^3)[a]	K_a[b]	inferred H/G stoichiometry
$B(p\text{-}C_6H_4Cl)_4^-$	386.8	$(2.16 \pm 0.05) \times 10^2$	1:4
$B(p\text{-}C_6H_4F)_4^-$	339.6	$(1.36 \pm 0.04) \times 10^2$	1:4
IO_4^-	64.2	$(5.73 \pm 0.32) \times 10^2$	1:2
ReO_4^-	77.3	$(5.98 \pm 0.33) \times 10^2$	1:2
$[PO_4(WO_3)_{12}]^{3-}$	692.4	–	1:1[c]

[a]Van der Waals volumes of anions based on the crystal structures (Table S5) were calculated by MoloVol.[31] [b]K_a (M^{-1}) were determined by ^{1}H NMR spectroscopy. [c]Bound by $Zn^{II}_6L_4$ cage **3**.

Given the size of the guest, we infer the guests to bind peripherally, at the four cage windows, in contrast to previously reported 1:1 peripheral binding of this guest to a different M_6L_4 cage with T symmetry.[11c]

The NMR titration data of guests $B(p\text{-}C_6H_4Cl)_4^-$ and $B(p\text{-}C_6H_4F)_4^-$ with **1** were plotted and fitted to the Hill function.[29] These anions displayed Hill coefficients of ca. 1.3 and 1.4, respectively, indicating a weakly cooperative binding mode (Figures S50–S53). The association constants for the $B(p\text{-}C_6H_4Cl)_4^-$ and $B(p\text{-}C_6H_4F)_4^-$ were determined to be 2.16×10^2 and 1.36×10^2 M^{-1}, respectively.

In contrast to the anionic guests $B(C_6H_5)_4^-$, $B(p\text{-}C_6H_4Cl)_4^-$, and $B(p\text{-}C_6H_4F)_4^-$, the more electron-deficient pentafluorophenyl and tetrakis[3,5-bis(trifluoromethyl)-phenyl] borates were not bound by **1** (Figures S50–S53, S59, and S63). We infer that the increased electron-deficiency of the polyfluorinated tetraphenylborates could prevent binding due to the weaker electrostatic interaction between these anionic guests and cationic host **1**.

The oxoanions IO_4^- and ReO_4^- bound with a 1:2 host–guest stoichiometry, with similar association constants of 5.73×10^2 and 5.98×10^2 M^{-1}, respectively (Figures S46–S49 and S54–S57). Noting that four equivalents of the peripherally binding larger anions $B(p\text{-}C_6H_4Cl)_4^-$ and $B(p\text{-}C_6H_4F)_4^-$ bound to **1**, we infer that the smaller ones ReO_4^- and IO_4^- bound internally. Two equivalents of these oxoanions fit easily within the cavity of **1** (Tables 1, S4, and S5),[30,31] and internal binding of similar anions was observed in related M_6L_4 species.[11c] As the volume of $[PO_4(WO_3)_{12}]^{3-}$ exceeds the cavity volume of **3** (Tables S4 and S5), we infer that this cluster is bound peripherally.

To further study the binding ability of **1** toward neutral guests, we treated the cage with polyaromatic hydrocarbons such as pyrene, corannulene, triphenylene, and dibenzo[g,p]chrysene, all of which were observed to bind to cage **1** in fast exchange on the NMR timescale (Figures S58 and S60–S62). However, the poor solubility of these guests precluded K_a determination.

CONCLUSIONS

Novel $Zn^{II}_9L_6$ tricapped trigonal prism and $Zn^{II}_6L_4$ structures with S_4 and D_2 symmetries thus establish the use of 8-aminoquinolines in subcomponent self–assembly of complex three-dimensional structures, beyond their use in copper(I) helicates.[32] These zinc(II) architectures bind a diverse array of guests, and show the ability to reconfigure to optimize guest binding. Such dynamic reconfiguration might enable the preparation of new classes of heteroleptic structures with lower symmetries,[33] capable of binding low-symmetry guests. Such species are potentially of interest in the purification of low-symmetry, complex molecules from mixtures.[4b]

ASSOCIATED CONTENT

Supporting Information

The Supporting Information is available free of charge at https://pubs.acs.org/doi/10.1021/jacs.3c03981.

Experimental procedures; NMR characterizations; mass spectrometry data; volume calculations; and X-ray crystallographic data (PDF)

Accession Codes

CCDC 2180301 contains the supplementary crystallographic data for this paper. These data can be obtained free of charge via www.ccdc.cam.ac.uk/data_request/cif, or by emailing data_request@ccdc.cam.ac.uk, or by contacting The Cambridge Crystallographic Data Centre, 12 Union Road, Cambridge CB2 1EZ, UK; fax: +44 1223 336033.

AUTHOR INFORMATION

Corresponding Author

Jonathan R. Nitschke – *Yusuf Hamied Department of Chemistry, University of Cambridge, Cambridge CB2 1EW, U.K.*; Email: jrn34@cam.ac.uk

https://doi.org/10.1021/jacs.3c03981
J. Am. Chem. Soc. 2023, 145, 15990–15996

Authors

Hua-Kui Liu − *Yusuf Hamied Department of Chemistry, University of Cambridge, Cambridge CB2 1EW, U.K.*

Tanya K. Ronson − *Yusuf Hamied Department of Chemistry, University of Cambridge, Cambridge CB2 1EW, U.K.;* orcid.org/0000-0002-6917-3685

Kai Wu − *Yusuf Hamied Department of Chemistry, University of Cambridge, Cambridge CB2 1EW, U.K.;* orcid.org/0000-0001-6336-7836

Dong Luo − *Yusuf Hamied Department of Chemistry, University of Cambridge, Cambridge CB2 1EW, U.K.*

Complete contact information is available at: https://pubs.acs.org/10.1021/jacs.3c03981

Author Contributions

The manuscript was written through contributions of all authors. All authors have given approval to the final version of the manuscript.

Notes

The authors declare no competing financial interest.

■ ACKNOWLEDGMENTS

This study was supported by the European Research Council (695009) and the UK Engineering and Physical Sciences Research Council (EPSRC, EP/T031603/1, and EP/P027067/1). H.K.L. thanks the Shanghai Institute of Organic Chemistry for a postdoctoral fellowship. We thank the Department of Chemistry NMR facility, University of Cambridge, for performing some NMR experiments and Diamond Light Source (UK) for the synchrotron beamtime on I19 (CY21497).

■ REFERENCES

(1) (a) Galan, A.; Ballester, P. Stabilization of reactive species by supramolecular encapsulation. *Chem. Soc. Rev.* **2016**, *45*, 1720−1737. (b) Wang, K.; Jordan, J. H.; Hu, X.-Y.; Wang, L. Supramolecular strategies for controlling reactivity within confined nanospaces. *Angew. Chem., Int. Ed.* **2020**, *59*, 13712−13721.

(2) (a) Mal, P.; Breiner, B.; Rissanen, K.; Nitschke, J. R. White phosphorus is air-stable within a self−assembled tetrahedral capsule. *Science* **2009**, *324*, 1697−1699. (b) Yamashina, M.; Sei, Y.; Akita, M.; Yoshizawa, M. Safe storage of radical initiators within a polyaromatic nanocapsule. *Nat. Commun.* **2014**, *5*, 4662.

(3) (a) Brzechwa-Chodzyńska, A.; Drożdż, W.; Harrowfield, J.; Stefankiewicz, A. R. Fluorescent sensors: a bright future for cages. *Coord. Chem. Rev.* **2021**, *434*, 213820. (b) Ahmad, N.; Younus, H. A.; Chughtai, A. H.; Verpoort, F. Metal−organic molecular cages: applications of biochemical implications. *Chem. Soc. Rev.* **2015**, *44*, 9−25. (c) Dhamija, A.; Das, C. K.; Ko, Y. H.; Kim, Y.; Mukhopadhyay, R. D.; Gunnam, A.; Yu, X.; Hwang, I.-C.; Schäfer, L. V.; Kim, K. Remotely controllable supramolecular rotor mounted inside a porphyrinic cage. *Chem* **2022**, *8*, 543−556. (d) Chan, A. K.; Lam, W. H.; Tanaka, Y.; Wong, K. M.; Yam, V. W. Multiaddressable molecular rectangles with reversible host−guest interactions: modulation of pH-controlled guest release and capture. *Proc. Natl. Acad. Sci. U.S.A.* **2015**, *112*, 690−695. (e) Zhang, Z.; Kim, D. S.; Lin, C. Y.; Zhang, H.; Lammer, A. D.; Lynch, V. M.; Popov, I.; Miljanic, O. S.; Anslyn, E. V.; Sessler, J. L. Expanded porphyrin-anion supramolecular assemblies: environmentally responsive sensors for organic solvents and anions. *J. Am. Chem. Soc.* **2015**, *137*, 7769−7774. (f) Custelcean, R.; Bonnesen, P. V.; Duncan, N. C.; Zhang, X.; Watson, L. A.; Van Berkel, G.; Parson, W. B.; Hay, B. P. Urea-functionalized M_4L_6 cage receptors: anion-templated self−assembly and selective guest exchange in aqueous solutions. *J. Am. Chem. Soc.* **2012**, *134*, 8525−8534. (g) Gemen, J.; Białek, M. J.; Kazes, M.; Shimon, L. J. W.; Feller, M.; Semenov, S. N.; Diskin-Posner, Y.; Oron, D.; Klajn, R. Ternary host−guest complexes with rapid exchange kinetics and photoswitchable fluorescence. *Chem* **2022**, *8*, 2362−2379.

(4) (a) Wu, K.; Li, K.; Hou, Y.-J.; Pan, M.; Zhang, L.-Y.; Chen, L.; Su, C.-Y. Homochiral D_4-symmetric metal−organic cages from stereogenic Ru(II) metalloligands for effective enantioseparation of atropisomeric molecules. *Nat. Commun.* **2016**, *7*, 10487. (b) Zhang, D.; Ronson, T. K.; Zou, Y.-Q.; Nitschke, J. R. Metal−organic cages for molecular separations. *Nat. Rev. Chem.* **2021**, *5*, 168−182. (c) Fuertes-Espinosa, C.; Pujals, M.; Ribas, X. Supramolecular purification and regioselective functionalization of fullerenes and endohedral metallofullerenes. *Chem* **2020**, *6*, 3219−3262. (d) Cui, P.-F.; Liu, X.-R.; Lin, Y.-J.; Li, Z.-H.; Jin, G.-X. Highly selective separation of benzene and cyclohexane in a spatially confined carborane metallacage. *J. Am. Chem. Soc.* **2022**, *144*, 6558−6565. (e) Fuertes-Espinosa, C.; Gómez-Torres, A.; Morales-Martínez, R.; Rodríguez-Fortea, A.; García-Simón, C.; Gándara, F.; Imaz, I.; Juanhuix, J.; Maspoch, D.; Poblet, J. M.; Echegoyen, L.; Ribas, X. Purification of Uranium-based endohedral metallofullerenes (EMFs) by selective supramolecular encapsulation and release. *Angew. Chem., Int. Ed.* **2018**, *57*, 11294−11299.

(5) (a) Takezawa, H.; Shitozawa, K.; Fujita, M. Enhanced reactivity of twisted amides inside a molecular cage. *Nat. Chem.* **2020**, *12*, 574−578. (b) Kaphan, D. M.; Levin, M. D.; Bergman, R. G.; Raymond, K. N.; Toste, F. D. A supramolecular microenvironment strategy for transition metal catalysis. *Science* **2015**, *350*, 1235−1238. (c) Heard, A. W.; Goldup, S. M. Synthesis of a mechanically planar chiral rotaxane ligand for enantioselective catalysis. *Chem* **2020**, *6*, 994−1006. (d) Li, T.-R.; Huck, F.; Piccini, G. M.; Tiefenbacher, K. Mimicry of the proton wire mechanism of enzymes inside a supramolecular capsule enables β-selective O-glycosylations. *Nat. Chem.* **2022**, *14*, 985−994. (e) Cullen, W.; Misuraca, M. C.; Hunter, C. A.; Williams, N. H.; Ward, M. D. Highly efficient catalysis of the Kemp elimination in the cavity of a cubic coordination cage. *Nat. Chem.* **2016**, *8*, 231−236. (f) Omagari, T.; Suzuki, A.; Akita, M.; Yoshizawa, M. Efficient catalytic epoxidation in water by axial N-ligand-free Mn-porphyrins within a micellar capsule. *J. Am. Chem. Soc.* **2016**, *138*, 499−502. (g) Zhao, L.; Jing, X.; Li, X.; Guo, X.; Zeng, L.; He, C.; Duan, C. Catalytic properties of chemical transformation within the confined pockets of Werner-type capsules. *Coord. Chem. Rev.* **2019**, *378*, 151−187. (h) Fang, Y.; Powell, J. A.; Li, E.; Wang, Q.; Perry, Z.; Kirchon, A.; Yang, X.; Xiao, Z.; Zhu, C.; Zhang, L.; Huang, F.; Zhou, H.-C. Catalytic reactions within the cavity of coordination cages. *Chem. Soc. Rev.* **2019**, *48*, 4707−4730. (i) Dhamija, A.; Gunnam, A.; Yu, X.; Lee, H.; Hwang, I.-C.; Ho Ko, Y.; Kim, K. Dramatically enhanced reactivity of fullerenes and tetrazine towards the inverse-electron-demand Diels−Alder reaction inside a porous porphyrinic cage. *Angew. Chem., Int. Ed.* **2022**, *134*, No. e202209326. (j) Chu, D.; Gong, W.; Jiang, H.; Tang, X.; Cui, Y.; Liu, Y. Boosting enantioselectivity of chiral molecular catalysts with supramolecular metal−organic cages. *CCS Chem.* **2022**, *4*, 1180−1189. (k) Olivo, G.; Capocasa, G.; Del Giudice, D.; Lanzalunga, O.; Di Stefano, S. New horizons for catalysis disclosed by supramolecular chemistry. *Chem. Soc. Rev.* **2021**, *50*, 7681−7724. (l) Gadzikwa, T.; Bellini, R.; Dekker, H. L.; Reek, J. N. H. Self−assembly of a confined rhodium catalyst for asymmetric hydroformylation of unfunctionalized internal alkenes. *J. Am. Chem. Soc.* **2012**, *134*, 2860−2863. (m) Yan, D.-N.; Cai, L.-X.; Cheng, P.-M.; Hu, S.-J.; Zhou, L.-P.; Sun, Q.-F. Photooxidase mimicking with adaptive coordination molecular capsules. *J. Am. Chem. Soc.* **2021**, *143*, 16087−16094. (n) Wang, J.; Young, T. A.; Duarte, F.; Lusby, P. J. Synergistic noncovalent catalysis facilitates base-free Michael addition. *J. Am. Chem. Soc.* **2020**, *142*, 17743−17750. (o) Samanta, D.; Mukherjee, S.; Patil, Y. P.; Mukherjee, P. S. Self−assembled Pd_6 open cage with triimidazole walls and the use of its confined nanospace for catalytic Knoevenagel- and Diels-Alder reactions in aqueous medium. *Chem.—Eur. J.* **2012**, *18*, 12322−12329.

(6) (a) Zhang, D.; Ronson, T. K.; Nitschke, J. R. Functional capsules via subcomponent self−assembly. *Acc. Chem. Res.* **2018**, *51*, 2423−2436. (b) Howson, S. E.; Bolhuis, A.; Brabec, V.; Clarkson, G. J.; Malina, J.; Rodger, A.; Scott, P. Optically pure, water-stable metallo-helical 'flexicate' assemblies with antibiotic activity. *Nat. Chem.* **2012**, *4*, 31−36. (c) Frischmann, P. D.; Kunz, V.; Wurthner, F. Bright fluorescence and host−guest sensing with a nanoscale M_4L_6 tetrahedron accessed by self−assembly of zinc-imine chelate vertices and perylene bisimide edges. *Angew. Chem., Int. Ed.* **2015**, *54*, 7285−7289. (d) Anhäuser, J.; Puttreddy, R.; Glanz, L.; Schneider, A.; Engeser, M.; Rissanen, K.; Lützen, A. Subcomponent self−assembly of a cyclic tetranuclear Fe^{II} helicate in a highly diastereoselective self−sorting manner. *Chem.—Eur. J.* **2019**, *25*, 12294−12297. (e) Sham, K. C.; Yiu, S. M.; Kwong, H. L. Dodecanuclear hexagonal-prismatic $M_{12}L_{18}$ coordination cages by subcomponent self−assembly. *Inorg. Chem.* **2013**, *52*, 5648−5650. (f) Young, M. C.; Holloway, L. R.; Johnson, A. M.; Hooley, R. J. A supramolecular sorting hat: stereocontrol in metal−ligand self−assembly by complementary hydrogen bonding. *Angew. Chem., Int. Ed.* **2014**, *53*, 9832−9836. (g) Ren, D.-H.; Qiu, D.; Pang, C.-Y.; Li, Z.; Gu, Z.-G. Chiral tetrahedral iron(II) cages: diastereoselective subcomponent self−assembly, structure interconversion and spin-crossover properties. *Chem. Commun.* **2015**, *51*, 788−791. (h) Yi, S.; Brega, V.; Captain, B.; Kaifer, A. E. Sulfate-templated self−assembly of new M_4L_6 tetrahedral metal−organic cages. *Chem. Commun.* **2012**, *48*, 10295−10297. (i) Domer, J.; Slootweg, J. C.; Hupka, F.; Lammertsma, K.; Hahn, F. E. Subcomponent assembly and transmetalation of dinuclear helicates. *Angew. Chem., Int. Ed.* **2010**, *49*, 6430−6433. (j) Lavendomme, R.; Ronson, T. K.; Nitschke, J. R. Metal and organic templates together control the size of covalent macrocycles and cages. *J. Am. Chem. Soc.* **2019**, *141*, 12147−12158. (k) Chen, L.-J.; Yang, H.-B.; Shionoya, M. Chiral metallosupramolecular architectures. *Chem. Soc. Rev.* **2017**, *46*, 2555−2576. (l) Lewing, D.; Koppetz, H.; Hahn, F. E. Reversible formation and transmetalation of Schiff-base complexes in subcomponent self−assembly reactions. *Inorg. Chem.* **2015**, *54*, 7653−7659.

(7) (a) Bilbeisi, R. A.; Clegg, J. K.; Elgrishi, N.; de Hatten, X.; Devillard, M.; Breiner, B.; Mal, P.; Nitschke, J. R. Subcomponent self−assembly and guest-binding properties of face-capped $Fe_4L_4^{8+}$ capsules. *J. Am. Chem. Soc.* **2012**, *134*, 5110−5119. (b) Hu, S.-J.; Guo, X.-Q.; Zhou, L.-P.; Yan, D.-N.; Cheng, P.-M.; Cai, L.-X.; Li, X.-Z.; Sun, Q.-F. Guest-driven self−assembly and chiral induction of photofunctional lanthanide tetrahedral cages. *J. Am. Chem. Soc.* **2022**, *144*, 4244−4253. (c) Fu, J.; Zheng, B.; Zhang, H.; Zhao, Y.; Zhang, D.; Zhang, W.; Yang, X.-J.; Wu, B. Chirality transcription in the anion-coordination-driven assembly of tetrahedral cages. *Chem. Commun.* **2020**, *56*, 2475−2478. (d) Yeh, R. M.; Xu, J.; Seeber, G.; Raymond, K. N. Large M_4L_4 ((M = Al(III), Ga(III), In(III), Ti(IV)) tetrahedral coordination cages: an extension of symmetry-based design. *Inorg. Chem.* **2005**, *44*, 6228−6239. (e) Li, Y.; Dong, J.; Gong, W.; Tang, X.; Liu, Y.; Cui, Y.; Liu, Y. Artificial biomolecular channels: enantioselective transmembrane transport of amino acids mediated by homochiral zirconium metal−organic cages. *J. Am. Chem. Soc.* **2021**, *143*, 20939−20951.

(8) (a) Meng, W.; Breiner, B.; Rissanen, K.; Thoburn, J. D.; Clegg, J. K.; Nitschke, J. R. A self−assembled M_8L_6 cubic cage that selectively encapsulates large aromatic guests. *Angew. Chem., Int. Ed.* **2011**, *50*, 3479−3483. (b) Otte, M.; Kuijpers, P. F.; Troeppner, O.; Ivanović-Burmazović, I.; Reek, J. N. H.; de Bruin, B. Encapsulated cobalt-porphyrin as a catalyst for size-selective radical-type cyclopropanation reactions. *Chem.—Eur. J.* **2014**, *20*, 4880−4884. (c) Zhou, X.-P.; Wu, Y.; Li, D. Polyhedral metal−imidazolate cages: control of self−assembly and cage to cage transformation. *J. Am. Chem. Soc.* **2013**, *135*, 16062−16065. (d) Browne, C.; Brenet, S.; Clegg, J. K.; Nitschke, J. R. Solvent-dependent host-guest chemistry of an Fe_8L_{12} cubic capsule. *Angew. Chem., Int. Ed.* **2013**, *52*, 1944−1948. (e) Zhou, X.-C.; Wu, L.-X.; Wang, X.-Z.; Lai, Y.-L.; Ge, Y.-Y.; Su, J.; Zhou, X.-P.; Li, D. Self−assembly of a $Pd_4Cu_8L_8$ cage for epoxidation of styrene and its derivatives. *Inorg. Chem.* **2022**, *61*, 5196−5200. (f) Luo, D.; Wu, L.-X.; Zhang, Y.; Huang, Y.-L.; Chen, X.-L.; Zhou, X.-P.; Li, D. Self−assembly of a photoluminescent metal−organic cage and its spontaneous aggregation in dilute solutions enabling time-dependent emission enhancement. *Sci. China: Chem.* **2022**, *65*, 1105−1111. (g) Yang, Y.; Jia, J.-H.; Pei, X.-L.; Zheng, H.; Nan, Z.-A.; Wang, Q.-M. Diastereoselective synthesis of *O*-symmetric heterometallic cubic cages. *Chem. Commun.* **2015**, *51*, 3804−3807.

(9) Examples of octahedral cages with O_h-symmetry. (b) and (d) are O_h-symmetry pseudo-octahedra. (a) Saha, R.; Ghosh, A. K.; Samajdar, R. N.; Mukherjee, P. S. Self−assembled Pd^{II}_6 molecular spheroids and their proton conduction property. *Inorg. Chem.* **2018**, *57*, 6540−6548. (b) Hiraoka, S.; Harano, K.; Shiro, M.; Ozawa, Y.; Yasuda, N.; Toriumi, K.; Shionoya, M. Isostructural coordination capsules for a series of 10 different d^5−d^{10} transition−metal ions. *Angew. Chem., Int. Ed.* **2006**, *45*, 6488−6491. (c) Samanta, D.; Mukherjee, P. S. Component selection in the self−assembly of palladium(II) nanocages and cage-to-cage transformations. *Chem.—Eur. J.* **2014**, *20*, 12483−12492. (d) Tessarolo, J.; Lee, H.; Sakuda, E.; Umakoshi, K.; Clever, G. H. Integrative assembly of heteroleptic tetrahedra controlled by backbone steric bulk. *J. Am. Chem. Soc.* **2021**, *143*, 6339−6344. (e) Jansze, S. M.; Severin, K. Palladium-based metal−ligand assemblies: the contrasting behavior upon addition of pyridine or acid. *J. Am. Chem. Soc.* **2019**, *141*, 815−819. (f) Wang, S.; Sawada, T.; Ohara, K.; Yamaguchi, K.; Fujita, M. Capsule−capsule conversion by guest encapsulation. *Angew. Chem., Int. Ed.* **2016**, *55*, 2063−2066. (g) Chand, D. K.; Biradha, K.; Fujita, M.; Sakamoto, S.; Yamaguchi, K. A molecular sphere of octahedral symmetry. *Chem. Commun.* **2002**, 2486−2487.

(10) Example of octahedral cages with T_d-symmetry Fujita, M.; Oguro, D.; Miyazawa, M.; Oka, H.; Yamaguchi, K.; Ogura, K. Self−assembly of ten molecules into nanometer-sized organic host frameworks. *Nature* **1995**, *378*, 469−471.

(11) Examples of octahedral cages with *T*-symmetry. (a) He, C.; Lin, Z.; He, Z.; Duan, C.; Xu, C.; Wang, Z.; Yan, C. Metal−tunable nanocages as artificial chemosensors. *Angew. Chem., Int. Ed.* **2008**, *47*, 877−881. (b) Chepelin, O.; Ujma, J.; Wu, X.; Slawin, A. M. Z.; Pitak, M. B.; Coles, S. J.; Michel, J.; Jones, A. C.; Barran, P. E.; Lusby, P. J. Luminescent, enantiopure, phenylatopyridine iridium-based coordination capsules. *J. Am. Chem. Soc.* **2012**, *134*, 19334−19337. (c) Rizzuto, F. J.; Wu, W. Y.; Ronson, T. K.; Nitschke, J. R. Peripheral templation generates an $M^{II}_6L_4$ guest-binding capsule. *Angew. Chem., Int. Ed.* **2016**, *55*, 7958−7962. (d) Carpenter, J. P.; Ronson, T. K.; Rizzuto, F. J.; Héliot, T.; Grice, P.; Nitschke, J. R. Incorporation of a phosphino(pyridine) subcomponent enables the formation of cages with homobimetallic and heterobimetallic vertices. *J. Am. Chem. Soc.* **2022**, *144*, 8467−8473. (e) Wei, Z.; Jing, X.; Yang, Y.; Yuan, J.; Liu, M.; He, C.; Duan, C. A platinum(II)-based molecular cage with aggregation-induced emission for enzymatic photocyclization of alkynylaniline. *Angew. Chem., Int. Ed.* **2022**, *62*, No. e202214577. (f) Li, K.; Zhang, L.-Y.; Yan, C.; Wei, S.-C.; Pan, M.; Zhang, L.; Su, C.-Y. Stepwise assembly of $Pd_6(RuL_3)_8$ nanoscale rhombododecahedral metal−organic cages via metalloligand strategy for guest trapping and protection. *J. Am. Chem. Soc.* **2014**, *136*, 4456−4459.

(12) (a) Yazaki, K.; Akita, M.; Prusty, S.; Chand, D. K.; Kikuchi, T.; Sato, H.; Yoshizawa, M. Polyaromatic molecular peanuts. *Nat. Commun.* **2017**, *8*, 15914. (b) Rizzuto, F.; Nitschke, J. R. Stereochemical plasticity modulates cooperative binding in a $Co^{II}_{12}L_6$ cuboctahedron. *Nat. Chem.* **2017**, *9*, 903−908.

(13) McTernan, C. T.; Davies, J. A.; Nitschke, J. R. Beyond platonic: how to build metal−organic polyhedra capable of binding low-symmetry, information-rich molecular cargoes. *Chem. Rev.* **2022**, *122*, 10393−10437.

(14) Rizzuto, F. J.; Carpenter, J. P.; Nitschke, J. R. Multisite binding of drugs and natural products in an entropically favorable, heteroleptic receptor. *J. Am. Chem. Soc.* **2019**, *141*, 9087−9095.

(15) Chen, B.; Holstein, J. J.; Horiuchi, S.; Hiller, W. G.; Clever, G. H. Pd(II) coordination sphere engineering: pyridine cages, quinoline

https://doi.org/10.1021/jacs.3c03981
J. Am. Chem. Soc. 2023, 145, 15990−15996

bowls, and heteroleptic pills binding one or two fullerenes. *J. Am. Chem. Soc.* **2019**, *141*, 8907−8913.
(16) (a) Brenner, W.; Ronson, T. K.; Nitschke, J. R. Separation and selective formation of fullerene adducts within an $M^{II}_8L_6$ cage. *J. Am. Chem. Soc.* **2017**, *139*, 75−78. (b) Huang, N.; Wang, K.; Drake, H.; Cai, P.; Pang, J.; Li, J.; Che, S.; Huang, L.; Wang, Q.; Zhou, H.-C. Tailor-made pyrazolide-based metal−organic frameworks for selective catalysis. *J. Am. Chem. Soc.* **2018**, *140*, 6383−6390.
(17) (a) Lewis, J. E. M.; Crowley, J. D. Metallo−supramolecular self−assembly with reduced-symmetry ligands. *ChemPlusChem* **2020**, *85*, 815−827. (b) Stephenson, A.; Argent, S. P.; Riis-Johannessen, T.; Tidmarsh, I. S.; Ward, M. D. Structures and dynamic behavior of large polyhedral coordination cages: An unusual cage-to-cage interconversion. *J. Am. Chem. Soc.* **2011**, *133*, 858−870.
(18) Zarra, S.; Clegg, J. K.; Nitschke, J. R. Selective assembly and disassembly of a water-soluble $Fe_{10}L_{15}$ prism. *Angew. Chem., Int. Ed.* **2013**, *52*, 4837−4840.
(19) (a) Zhang, D.; Ronson, T. K.; Mosquera, J.; Martinez, A.; Guy, L.; Nitschke, J. R. Anion binding in water drives structural adaptation in an azaphosphatrane-functionalized $Fe^{II}_4L_4$ tetrahedron. *J. Am. Chem. Soc.* **2017**, *139*, 6574−6577. (b) Riddell, I. A.; Smulders, M. M. J.; Clegg, J. K.; Hristova, Y. R.; Breiner, B.; Thoburn, J. D.; Nitschke, J. R. Anion-induced reconstitution of a self−assembling system to express a chloride-binding $Co_{10}L_{15}$ pentagonal prism. *Nat. Chem.* **2012**, *4*, 751−756.
(20) (a) Hardy, M.; Struch, N.; Holstein, J. J.; Schnakenburg, G.; Wagner, N.; Engeser, M.; Beck, J.; Clever, G. H.; Lützen, A. Dynamic complex-to-complex transformations of heterobimetallic systems influence the cage structure or spin state of iron(II) ions. *Angew. Chem., Int. Ed.* **2020**, *59*, 3195−3200. (b) Tranchemontagne, D. J.; Ni, Z.; O'Keeffe, M.; Yaghi, O. M. Reticular chemistry of metal−organic polyhedra. *Angew. Chem., Int. Ed.* **2008**, *47*, 5136−5147.
(21) (a) McTernan, C. T.; Ronson, T. K.; Nitschke, J. R. Selective anion binding drives the formation of AgI_8L_6 and $AgI_{12}L_6$ six-stranded helicates. *J. Am. Chem. Soc.* **2021**, *143*, 664−670. (b) Carpenter, J. P.; McTernan, C. T.; Ronson, T. K.; Nitschke, J. R. Anion pairs template a trigonal prism with disilver vertices. *J. Am. Chem. Soc.* **2019**, *141*, 11409−11413.
(22) (a) Lang et. al. reportd low-symmetry vetices constructed octahedral metal organic cage which has a regular internal octahedral cavity. Bao, S.-J.; Xu, Z.-M.; Ju, Y.; Song, Y.-L.; Wang, H.; Niu, Z.; Li, X.; Braunstein, P.; Lang, J.-P. The covalent and coordination Co-driven assembly of supramolecular octahedral cages with controllable degree of distortion. *J. Am. Chem. Soc.* **2020**, *142*, 13356−13361. (b) Jin et. al. used two kind of vertices to build one C_1-symmetry octahedral cage. Liu, J.-J.; Lin, Y.-J.; Li, Z.-H.; Jin, G.-X. Self−assembled half-sandwich polyhedral cages via flexible schiff-base ligands: an unusual macrocycle-to-cage conversion. *Dalton Trans.* **2016**, *45*, 13675−13679. (c) Howlader, P.; Mondal, S.; Ahmed, S.; Mukherjee, P. S. Guest-induced enantioselective self−assembly of a Pd_6 homochiral octahedral cage with a C_3-symmetric pyridyl donor. *J. Am. Chem. Soc.* **2020**, *142*, 20968−20972.
(23) Stewart, J. J. P. MOPAC2016; Stewart Computational Chemistry: Colorado Springs, CO, USA, http://openmopac.net/MOPAC2016.html (accessed June 7, 2023).
(24) Fujitsu Ltd. *SCIGRESS*: Tokyo, Japan, 2013. (b) Stewart, J. J. P. Optimization of parameters for semiempirical methods V: modification of NDDO approximations and application to 70 elements. *J. Mol. Model.* **2007**, *13*, 1173−1213.
(25) Zhang, D.; Ronson, T. K.; Güryel, S.; Thoburn, J. D.; Wales, D. J.; Nitschke, J. R. Temperature controls guest uptake and release from Zn_4L_4 tetrahedra. *J. Am. Chem. Soc.* **2019**, *141*, 14534−14538.
(26) Given the ability of the template **G** to convert **2** to a single diastereomer of octahedron **3** with an S_4 symmetry, we investigated whether cage **1** with a mixture of S_4 and D_2 symmetry could also be converted into a single diastereomer of octahedron with an S_4 symmetry. Experiments using **G** as a template resulted in precipitation under the same condition described above for the conversion between $Zn^{II}_9L_6$ and $Zn^{II}_6L_4$, presumbly due to the poor solubility of the host−guest complex without the methyl group.
(27) CCDC 2180301 contains the supplementary crystallographic data for this paper. These data can be obtained free of charge from The Cambridge Crystallographic Data Center.
(28) Takezawa, H.; Murase, T.; Resnati, G.; Metrangolo, P.; Fujita, M. Recognition of polyfluorinated compounds through self−aggregation in a cavity. *J. Am. Chem. Soc.* **2014**, *136*, 1786−1788.
(29) Yang, D.; Greenfield, J. L.; Ronson, T. K.; von Krbek, L. K. S.; Yu, L.; Nitschke, J. R. La^{III} and Zn^{II} cooperatively template a metal−organic capsule. *J. Am. Chem. Soc.* **2020**, *142*, 19856−19861.
(30) We calculated the Van der Waals volumes using the MoloVol program, referring to the reported crystal structures of anions including $B(p\text{-}C_6H_4Cl)_4^-$ (CCDC, 748991), $B(p\text{-}C_6H_4F)_4^-$ (708376), IO_4^- (2168128), ReO_4^- (821877), $PO_4(WO_3)_{12}^{3-}$ (789283) based on the crystallographic data from The Cambridge Crystallographic Data Center. The caculated internal cavities of **1**-S_4, **1**-D_2, and crystal **3**-S_4 are 411.0, 452.7 and 558.9 Å^3, respectively.
(31) Maglic, J. B.; Lavendomme, R. MoloVol: an easy-to-use program for analyzing cavities, volumes and surface areas of chemical structures. *J. Appl. Crystallogr.* **2022**, *55*, 1033−1044.
(32) Hutin, M.; Bernardinelli, G.; Nitschke, J. R. Synthetic selectivity through avoidance of valence frustration. *Proc. Natl. Acad. Sci. U.S.A.* **2006**, *103*, 17655−17660.
(33) Ronson, T. K.; Carpenter, J. P.; Nitschke, J. R. Dynamic optimization of guest binding in a library of diastereomeric heteroleptic coordination cages. *Chem* **2022**, *8*, 557−568.

https://doi.org/10.1021/jacs.3c03981
J. Am. Chem. Soc. 2023, 145, 15990−15996